Template synthesis of porous nanoZnO and its adsorption capability

Congda Jiao, Fan Tang, Maoquan Xue ✉

Department of Mechanical Engineering, Changzhou Vocational Institute of Light Industry, Changzhou 213164, Jiangsu, People's Republic of China
✉ *E-mail: xuemaoq@163.com*

Published in Micro & Nano Letters; Received on 22nd January 2017; Revised on 28th February 2017; Accepted on 9th March 2017

Porous nanozinc oxide (ZnO) was successfully fabricated by a facile infiltration and calcination method with the help of a China rose petal template. The as-prepared products were studied by X-ray powder diffraction, field-emission scanning electron microscopy, and transmission electron microscopy (TEM). X-ray diffraction results proved that the as-prepared product was the hexagonal phase of ZnO without any impurity. Both SEM and TEM images showed that the biomorphic structures of ZnO were constructed with many regular nanoparticles with diameter of about 20 nm. The as-synthesised porous nanoZnO displayed excellent waste water treatment performance with high removal capacities toward methyl orange. This novel biotemplate process provides an economical and environmentally friendly route to obtain advanced assembling biomorphic nanoarchitectures, and will make it possible for their potential application in the field of catalysis and other.

1. Introduction: Zinc oxide (ZnO) is one of the most intensively researched materials because of its wide direct bandgap of 3.37 eV and large exciton binding energy of 60 meV at room temperature, which offer its promising applications in semiconductor devices, solar cells, field effect tube, piezoelectric material, gas sensors, detector, biosensors [1–3], etc.

The porous nanostructure of this material has important effects on its distinct properties, and the much available morphology can admit optimisation of its performances for peculiar applications such as photocatalysis, sensors, and photoelectrochemical cells [4, 5]. Herein, synthesis of porous nanoZnO using thermal evaporation method [6], electrochemical process [7], hydrothermal treatment [8, 9], aqueous sol–gel soaking [10], and calcining the Zn hydroxide carbonate precursor [11] is reported.

Biont in the nature have evolved over billions of years to produce multifarious efficient functions, for instance absorbent refining, self-cleaning, superhydrophobicity, light absorption, and mechanical reinforcement [12]. In these functions, the natural biomaterials with ideal micro/nanostructures such as butterfly wing, lotus leave, moths eyes, conch, petal, and leaf always play very significant roles. The genetic porous and hierarchical structures appear in biomaterials have been ascribed to their high surface area, light weight, large specific extended elasticity, and high permeability. When grasping the formation rules of these natural biomaterials and understanding their relationships between structure and function, we can start simulating and designing novel structural and functional materials.

Using natural biomaterials as templates, novel biomorphic products with charming designs could be fabricated for actual industrial applications [13–18]. China rose is perennial low shrub, belongs to the Rosaceae family. Its petal consists of unique subuliform secretory cells, and provides a powerful, hierarchical layered network structure, in addition to its extraordinary chemical and physical stability, makes the petal a perfect carrier for inorganic assembly. To the best of the authors' knowledge, synthesis of porous ZnO using natural petal as template has seldom been reported. Herein, we chose an advantageous biomaterial China rose petal as the biotemplate to fabricate hierarchical ZnO by a solution immersion method followed by thermal decomposition. Then, the as-prepared porous nanoZnO were analysed using X-ray powder diffraction (XRD), scanning electron microscopy (SEM), and transmission electron microscopy (TEM), and the adsorption property of the porous ZnO on methyl orange removal were investigated.

2. Experimental methods

2.1. Synthesis of biomorphic ZnO nanostructures: All chemical reagents were analytically pure, purchased from commercial sources directly, and used without purification. Fresh rose petals were picked from garden.

In a typical procedure, 5 g fresh China rose petals were washed several times with deionised water to remove floating dust, and then immersed in water/ethanol mixture to modify cell wall of petal, in order to make it more easily react with Zn chloride ($ZnCl_2$).

The pH value of the mixture was adjusted to 4 by HCl and soaked about 1 h, and then 4 g $ZnCl_2$ was added to the above mixture and continuously magnetic stirred. The Zn ions infiltrated into petal cell wall for 24 h at room temperature. After endosmosis, the petals were collected followed by washing several times with distilled water and dried in a drying oven for 24 h at 60°C. Finally, the templated hybrids were then placed in an alundum crucible, and calcined for 2 h at 550°C and cooled to room temperature naturally in air.

2.2. Characterisation: The X-ray diffraction patterns were performed on a D8 advance (Bruker-AXS) diffractometer under copper (Cu) Kα radiation ($\lambda = 0.1546$ nm). The morphologies and structures of the samples were investigated by an SEM (SEM, Japan Electron Optics Laboratory (JEOL) JXA-840A) and a TEM (TEM, JEOL JEM-100CX II) using an accelerating voltage of 200 kV. The specimens for the SEM analysis were prepared by placing the ZnO powders on to a Cu disc with conducting resin followed by metal spraying. The specimens for the TEM studies were prepared by suspending the powders in ethanol through ultra-sonication for 5 min and placing a drop on a carbon-coated Cu grid. All the measurements were carried out at room temperature.

The thermogravimetric (TG) and differential scanning calorimetry (DSC) curves of the petal-templated hybrid were recorded on an instruments analyser (NETZSCH-Ger tebau Gesellschaft mit beschrankter Haftung (GmbH) Selb/Germany) under the oxygen atmosphere (the heating was 10°C/min).

2.3. Adsorption experiment: To assess the adsorption performance of the as-prepared porous ZnO, the as-synthesised porous nanoZnO was used to remove methyl orange from aqueous solution. About 20 mg porous ZnO were added into 100 ml methyl orange solution. Then, the suspension was mechanically shaken at a constant speed. After adsorption for 1 h, some specimens (5 ml) were taken from the suspension and centrifuged to remove the

doi: 10.1049/mnl.2017.0014

adsorbent. The supernatant solutions were studied by using ultraviolet–visible spectroscopy to gain the methyl orange concentrations in the solution.

3. Results and discussion: Fig. 1*a* shows the XRD of fresh China rose petals after being washed, it did not detect the inorganic crystals, means that all possible contaminants on surface of petals have been cleaned, and there is no other impurity. The crystalline structure and phase purity of the synthesised products after calcination were also verified by XRD. As shown in Fig. 1*b*, all observed diffraction peaks can be systematically indexed to those of the hexagonal phase of ZnO, which are consistent with the values in the standard card (JCPDS Card No. 36–1451). No other impurity peaks are detected in the XRD pattern, indicating that petal templates were completely removed and the sample was highly crystalline.

The formation of hierarchical ZnO was traced from the calcination process by carrying out TG and DSC research. The corresponding curves of petal-templated hybrids are shown in Fig. 2. It is explicit that the hybrids start decomposed at about 200°C, the petals template are completely removed at 500°C, only remained 36% inorganic matters. In addition, DSC curve shows two peaks around 310 and 462°C with an interval about 150°C, which indicated the synthesis of biomorphic ZnO has experienced two stages. It is believed that the weight loss between 250 and 360°C due to the thermal decomposition and carbonisation of the organic petals. The following weight loss till 500°C is considered to the complete combustion of those carbonised products.

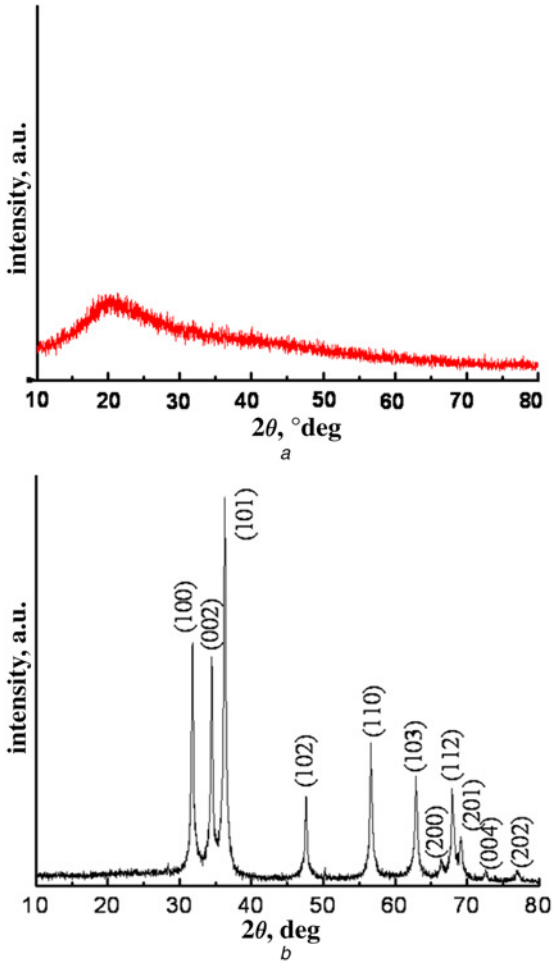

Fig. 1 *XRD pattern*
a Fresh China rose petals
b As-prepared nanoZnO

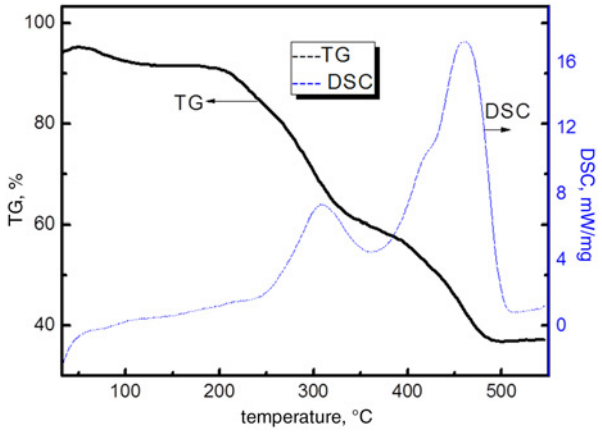

Fig. 2 *TG and DSC curves of the petal-templated hybrids*

Therefore, it is advisable for calcination to remove the petals template at 550°C.

China rose is known as the queen of flower, it is an evergreen, bushy plant. The type of China rose is variety, have single-lobe or polyphyll, and often quite irregular in outline, its colour ranges from milky white to dark red. Its petal is composed of epidermis, parenchyma, and vascular tissue, the parenchyma contains many oil cells, and epidermis has unique papillae secretory cells and provides a powerful, hierarchical porous network structure. Fig. 3*a* shows a petals fully opened flower blooming on a stem. The morphology and structure of the samples is studied using field-emission SEM. Fig. 3*b* displays the fresh China rose petal preprocessed through immersion in $HCl/ZnCl_2$ solution is

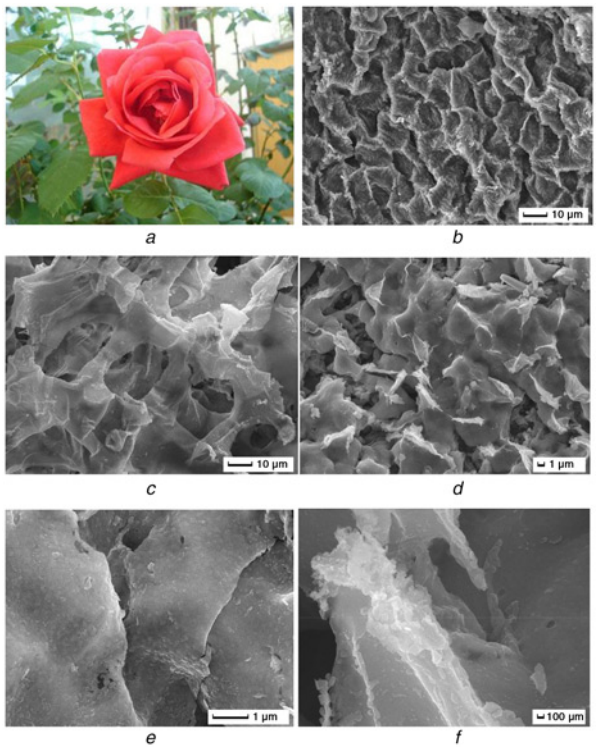

Fig. 3 *Petals fully opened flower blooming on a stem*
a Photograph of China rose
b Surface of original China rose petal pretreated by soaking in $ZnCl_2$ solution
c Subcutaneous tissue of original China rose petal pretreated by soaking in $ZnCl_2$ solution
d Full view of SEM images of hierarchical ZnO fabricated at 550°C
e, *f* Higher magnification of image (d)

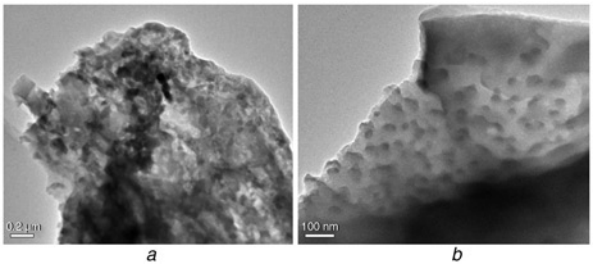

Fig. 4 *TEM images of*
a Fracted ZnO with the structure of petal cell
b Edge of nanoZnO

composed of microcraters. The diameters of craters vary from 8 to 10 μm. Fig. 3*c* shows subcutaneous tissue structure of petals by immersion in $HCl/ZnCl_2$ solution, it is obvious that the vascular fibres with porous structure have average width from nanoscale to the micrometre scale with mutual cross-linked three-dimensional natural biological structure. Fig. 3*d* shows the microstructures of biomorphic ZnO calcined at 550°C in air. The surface of the sample distributes periodic array of subuliform convex, which is similar to that of the supernormal microstructure of original rose petal surface. Calcination reduced the rose petal cells. It is obvious in Fig. 3*e* that the nanoZnOs are rough and porous. Higher magnification SEM image in Fig. 3*f* more clearly reveals the porous structure in the respective nanoZnO. It makes clear that the as-prepared ZnO shown well duplication quality for both micro and nanosized surface features of the original petal.

Transmission electron microscopy images (Figs. 4*a* and *b*) provide further insight into the morphologies and microstructures of the as-prepared biomorphic nanoZnO. It can be seen that the lamella in Figs. 3*d–f* is composed of multilayer ultrathin nanometre layer, each layer is constituted of ZnO polycrystalline nanoparticles, and form a large number of nanopores, the whole structure is like a multilayer transparent paper. Therefore, the nanoZnO successfully reproduces the hierarchical structure cell wall of the original petal template. After calcination, the hierarchical structures are still retained, and there is no collapse in the structures. The TEM image derived from the edge of nanoZnO (Fig. 4*b*) indicated that the layered lamella consists of nanoparticles.

The Brunauer–Emmett–Teller (BET) surface area of porous nanoZnO calculated by the BET method is 55.9 $m^2 g^{-1}$. As-synthesised porous nanoZnO with a high special surface area, which provides more surface active sites and pore-channels for the adsorptions and diffusion of reactants [17].

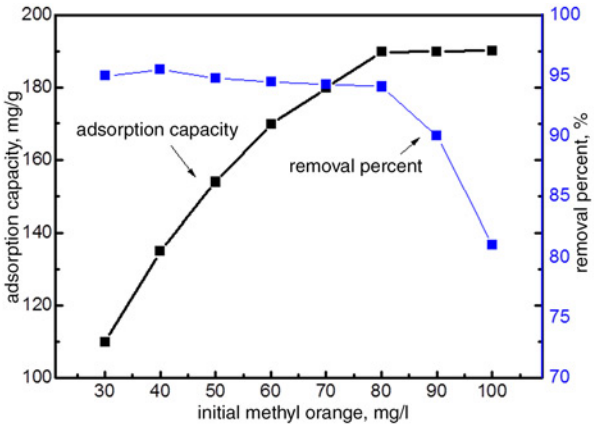

Fig. 5 *Adsorption isotherm and removal per cent of methyl orange by the as-prepared porous nanoZnO*

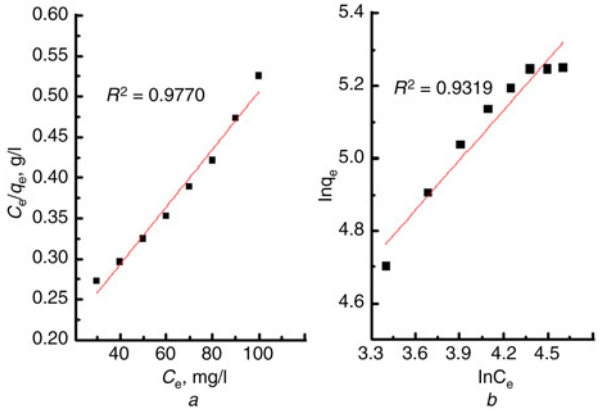

Fig. 6 *Equilibrium isotherm for methyl orange adsorbed by porous nanoZnO*
a Langmuir model
b Freundlich model

Fig. 5 shows the effect of initial methyl orange concentration on the adsorption capacity and removal per cent of the prepared porous nanoZnO. It was shown that the adsorption capacity of methyl orange increases quickly and almost linearly growth from 110.05 to 189.87 mg/g increased with the increase in initial methyl orange concentration in the interval from 30 to 80 mg/l, which manifests that there have been a large number of easily available adsorption sites under low concentration. With further increasing concentration, the growth trend of removal ability becomes slow. This maybe due to the reduced adsorption sites being available at the end of the adsorption process and the difficulty of methyl orange diffusion into the micropores on the porous ZnO.

The removal per cent reduced with increasing initial concentration of methyl orange. The removal percentage of methyl orange slowly decreased when initial concentration of methyl orange was <80 mg/l, but it maintained more than 94.15%. When further increasing concentration of methyl orange, the removal percentage decreased sharply. A possible explanation is that the adsorption sites on the porous ZnO were not fully occupied at a low concentration of methyl orange, thus the adsorption capacity of methyl orange increased and the removal percentage change was not obvious [19–21]. When the concentration of methyl orange solution was higher, the number of methyl orange molecule was beyond the adsorption ability of the porous ZnO, so the decreasing trend of methyl orange removal became speedy.

To study the adsorption mechanism of methyl orange on the prepared porous nanoZnO adsorbent, Langmuir and Freundlich adsorption isotherms models were applied to study the equilibrium adsorption data of methyl orange on the prepared adsorbent, Langmuir adsorption isotherm is based on the assumption that monolayer adsorption occurs on a homogeneous surface; while Freundlich adsorption isotherm is based on the assumption over a heterogeneous surface, the Langmuir and Freundlich isotherms models are according to previous studies [19, 22, 23]. From Fig. 6, it can be concluded that the adsorption isotherm of methyl orange can be described well by the Langmuir model rather than Freundlich model (R^2 was 0.9770 and 0.9319 for Langmuir and Freundlich fit, respectively), which indicates that a monolayer adsorption between the porous nanoZnO and the methyl orange occurs [19, 22].

4. Conclusion: In summary, biomorphic porous nanoZnO were successfully fabricated by a China rose petal-assisted infiltration and calcination process under green, economical and easy method. The experimental results show that the porous nanoZnO product is formed via an infiltration–combination–decomposition

doi: 10.1049/mnl.2017.0014

process. It is our hope that this inexpensive, efficient, and environment-friendly synthetic method can be used as a universal method for the preparation of other transition metal–oxide porous biomorphic nano or micromaterials. The as-synthesised porous nanoZnO exhibited excellent adsorption capacities to methyl orange.

5. Acknowledgment: This work was supported by the Innovation Training Programs for Undergraduates of Jiangsu Province (201613101006Y) and Qinglan Project of Jiangsu Province.

6 References

[1] Ye Y., Guo T.L., Jiang Y.D.: 'Field emission from ZnO nanostructures prepared by electrodeposition', *Mater. Technol.*, 2012, **27**, (4), pp. 205–299

[2] Fouad O.A., Glaspell G., El-Shall M.S.: 'Structural, optical and gas sensing properties of ZnO, SnO_2 and ZTO nanostructures', *Nano*, 2010, **5**, (04), pp. 185–194

[3] Purushothaman K.K., Suba Priya V., Nagamuthu S.: 'Synthesising of ZnO nanopetals for supercapacitor applications', *Micro Nano Lett.*, 2011, **6**, (8), pp. 668–670

[4] Sun Y., Zhang Y., Xu Y.: 'Synthesis and visible-light photocatalytic properties of ZnO flake-like ensembles', *Micro Nano Lett.*, 2012, **7**, (11), pp. 1147–1150

[5] Kumar P.S., Paik P., Raj A.D.: 'Biodegradability study and pH influence on growth and orientation of ZnO nanorods via aqueous solution process', *Appl. Surf. Sci.*, 2012, **258**, (18), pp. 6765–6771

[6] Zhang J., Deng S.J., Liu Y.: 'Preparation and photocatalytic activity of Nd doped ZnO nanoparticles', *Mater. Technol.*, 2014, **29**, (5), pp. 262–268

[7] Subramanian N., Amal A.G.: 'A green synthetic route for zinc oxide nanoarchitectures using l-lysine', *Mater. Lett.*, 2013, **92**, pp. 361–364

[8] Hou Q., Zhu L., Chen H.: 'Growth of porous ZnO nanosheets by electrodeposition with $Zn_4SO_4(OH)_6{\cdot}4H_2O$ as precursor', *Electrochim. Acta*, 2012, **85**, pp. 438–443

[9] Li S., Zhang X., Jiao X.: 'One-step large-scale synthesis of porous ZnO nanofibers and their application in dye-sensitized solar cells', *Mater. Lett.*, 2011, **65**, (19), pp. 2975–2978

[10] Sirimanne P.M., Premalal E.V.A., Minoura H.: 'Sensitization of nano-porous ZnO photo-anode by a conjugated conducting polymer', *Renew. Energy*, 2011, **36**, (1), pp. 405–408

[11] Wang X., Cai W., Liu S.: 'ZnO hollow microspheres with exposed porous nanosheets surface: structurally enhanced adsorption towards heavy metal ions', *Colloids Surf. A, Physicochem. Eng. Aspects*, 2013, **422**, pp. 199–205

[12] Promnimit S., Baruah S., Lamdu U.: 'Hydrothermal growth of ZnO hexagonal nanocrystals: effect of growth conditions', *J. Nano Res.*, 2013, **21**, pp. 57–63

[13] Fatemi H., Khodadadi A.A., Anaraki F.A.: 'Apple–biomorphic synthesis of porous ZnO nanostructures for glucose direct electrochemical biosensor', *Curr. Appl. Phys.*, 2012, **12**, (4), pp. 1033–1038

[14] Lei A., Qu B., Zhou W.: 'Facile synthesis and enhanced photocatalytic activity of hierarchical porous ZnO microspheres', *Mater. Lett.*, 2012, **66**, (1), pp. 72–75

[15] Liu Q., Gao L., Jiang L.: 'Biomimetic preparation and multi-scale microstructures of nano-silica/polyurethane elastomeric fibers', *Prog. Nat. Sci., Mater. Int.*, 2013, **23**, (6), pp. 532–542

[16] Li J., Kwong F.L., Zhu J.: 'Synthesis of biomorphic ZnO nanostructures by using the cetyltrimethylammonium bromide modified silk templates', *J. Am. Ceram. Soc.*, 2010, **93**, (11), pp. 3726–3731

[17] Qian J., Chen F., Zhao X.: 'China rose petal as biotemplate to produce two-dimensional ceria nanosheets', *J. Nanoparticle Res.*, 2011, **13**, (12), pp. 7149–7158

[18] Sifontes A.B., Gonzalez G., Ochoa J.L.: 'Chitosan as template for the synthesis of ceria nanoparticles', *Mater. Res. Bull.*, 2011, **46**, (11), pp. 1794–1799

[19] Song H.J., You S.S., Jia X.H.: 'Synthesis of fungus-like MoS_2 nanosheets with ultrafast adsorption capacities toward organic dyes', *Appl. Phys. A*, 2015, **121**, (2), pp. 541–548

[20] Sun X.F., Liu B., Jing Z., *ET AL.*: 'Preparation and adsorption property of xylan/poly (acrylic acid) magnetic nanocomposite hydrogel adsorbent', *Carbohydr. Polym.*, 2015, **118**, pp. 16–23

[21] Yu X.F., Liu J.W., Cong H.P.: 'Template- and surfactant-free synthesis of ultrathin CeO_2 nanowires in a mixed solvent and their superior adsorption capability for water treatment', *Chem. Sci.*, 2015, **6**, (4), pp. 2511–2515

[22] Yang Y., Teng F., Kan Y.: 'Controllable synthesis of 'L'-shaped V_2O_5 and the improved adsorption capacity by fluorine', *Cryst. Eng. Commun.*, 2016, **18**, (17), pp. 3064–3078

[23] Wang S., Teng F., Zhao Y.: 'Effect of the molecular structure and surface charge of a bismuth catalyst on the adsorption and photocatalytic degradation of dye mixtures', *RSC Adv.*, 2015, **5**, (93), pp. 76588–76598